

## A statistical analysis of ionospheric velocity and magnetic field power spectra at the time of pulsed ionospheric flows

G. A. Abel and M. P. Freeman

British Antarctic Survey, Natural Environment Research Council, Cambridge, UK

Received 22 March 2002; revised 8 July 2002; accepted 13 August 2002; published 24 December 2002.

[1] We analyze the power spectrum of the line-of-sight ionospheric velocity measured by the SuperDARN CUTLASS Finland radar and of contemporaneous magnetic field perturbations measured by nearby IMAGE magnetometers. The measurements come from 69–87° AACGM latitude and 0415–2230 MLT during 58 intervals of pulsed ionospheric flow between March 1995 and September 1996. The median power spectrum of both the velocity and magnetic field is of power law form with a best fit exponent of  $-0.5$  and  $-1.3$ , respectively. By simulating the effect of the finite sample window on the measured spectral exponent and on the structure seen in the power spectral density of individual spectra, we show that the measured spectral exponent actually corresponds to a true exponent of  $-0.95$  for the velocity and  $-1.8$  for the magnetic field. Furthermore, it is shown that the difference in the exponents of the velocity and magnetic field spectra is at least in part due to a spatial smoothing effect that causes the spectral exponent of the ground magnetic spectrum to be less than that of the ionospheric current spectrum producing it. The power law power spectrum implies that there is no preferred timescale for ionospheric velocity and current fluctuations in the observed frequency range. It is proposed that this scale-free nature may arise from the intermittent, turbulent nature of the interplanetary magnetic field causing magnetic reconnection to occur at the magnetopause on a wide range of spatial and temporal scales. *INDEX TERMS*: 2760 Magnetospheric Physics: Plasma convection; 2437 Ionosphere: Ionospheric dynamics; 2784 Magnetospheric Physics: Solar wind/magnetosphere interactions; 3250 Mathematical Geophysics: Fractals and multifractals; *KEYWORDS*: convection, reconnection, power spectrum

**Citation:** Abel, G. A., and M. P. Freeman, A statistical analysis of ionospheric velocity and magnetic field power spectra at the time of pulsed ionospheric flows, *J. Geophys. Res.*, 107(A12), 1470, doi:10.1029/2002JA009402, 2002.

### 1. Introduction

[2] The prime mechanism of energy transfer between the solar wind and the magnetosphere-ionosphere (M-I) system is through magnetic reconnection at the magnetopause. On system-wide temporal and spatial scales this mechanism and the general relationship between the solar wind and the M-I system is largely understood, both theoretically and observationally, and many facets of it can be accurately reproduced by MHD simulation in which the solar wind is a laminar flow. However, we understand much less well, either theoretically, observationally, or by numerical simulation, the spatiotemporal structure of magnetopause reconnection and the relationship between the solar wind and the M-I system on sub-system scales.

[3] The temporal behavior of magnetic reconnection at the magnetopause has been examined through the study of flux transfer events (FTEs) observed by in situ spacecraft. FTEs are thought to be transient reconnection events at the magnetopause. The distribution of recurrence times between FTEs has been shown to be a monotonically decreasing

function over timescales from 3 to  $\sim 30$  min [Lockwood and Wild, 1993; Kuo *et al.*, 1995]. The functional form of this distribution was not investigated but we find it to be a power law, i.e.,  $p = \tau^{-\beta}$  where  $p$  is the probability of interevent interval  $\tau$ . This is demonstrated in Figure 1 which shows the inter-FTE distributions found by Lockwood and Wild [1993] (solid line) and Kuo *et al.* [1995] (dotted line) on a log-log plot. A power law form (straight line) is seen over most of the observed range with similar power law exponents  $\sim 1.4$ .

[4] Further studies have looked at the temporal behavior of ionospheric signatures related to magnetopause reconnection. McWilliams *et al.* [2000] showed that the distributions of inter-FTE intervals were also similar to those of poleward moving auroral forms (PMAFs) observed by Fasel [1995] and of pulsed ionospheric flows (PIFs) that McWilliams *et al.* [2000] identified in SuperDARN radar data. These distributions are shown in Figure 1 by the dashed (PMAFs) and the dot-dashed (PIFs) lines, respectively. The observation of PMAFs is associated with the exceedance of some threshold in the appropriate time series, while in the case of PIFs, the situation is more complicated. McWilliams *et al.* [2000] derived their distribution of interflow burst intervals by (1) calculating the power spectra of

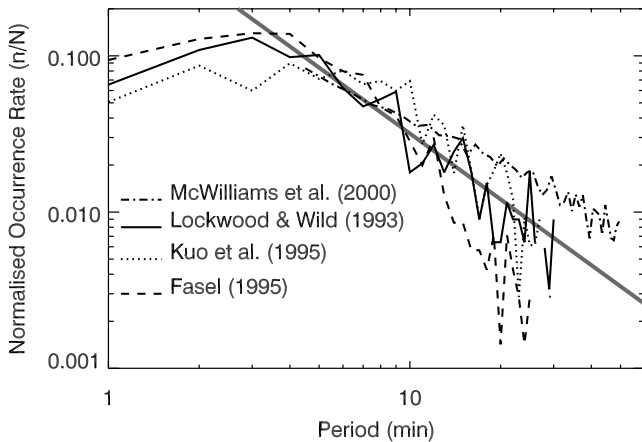


**Figure 1.** The occurrence rate of LOS velocity fluctuation periods at the time of PIFs as measured by *McWilliams et al.* [2000] (dot-dashed line) compared with distributions of inter-FTE intervals found in ISSE spacecraft data in the vicinity of dayside reconnection (*Lockwood and Wild* [1993] (solid line) and *Kuo et al.* [1995] (dotted line)) and the distribution of the time between ground-based optical measurements of PMAFs [*Fasel*, 1995] (dashed line). The grey straight line indicates a power law with  $\alpha = 1.4$ .

many sample intervals, (2) identifying each frequency  $f$  whose normalized power spectral density (PSD)  $P$  exceeded a noise threshold, and (3) calculating the occurrence frequency of the corresponding repetition periods, weighting each occurrence by the interval length and  $P$ . The resultant quantity was in reality more akin to a power spectrum than the occurrence frequency of repetition periods intended.

[5] Power law power spectra (i.e.,  $P = f^{-\alpha}$ ) in a similar frequency range have been reported in a number of studies of ground-based magnetic fluctuations, which are mainly due to ionospheric currents. The results of these studies are summarized in Table 1. In the largest such study, using 123 data years from 64 geomagnetic observatories over a wide range of latitudes and longitudes, *Campbell* [1976] concluded that the power spectra from individual observatories in the period range from 5 min to 4 hours (0.07–

3.3 mHz) were mostly power law in form with an exponent range  $1 \leq \alpha \leq 4.0$ , but usually  $\alpha \approx 2.0$ , and that no consistent frequency location for spectral peaks was observed.

[6] The fact that the M-I interevent interval distributions and power spectra are power law-like is interesting. They share the important property of statistical self-similarity. This means that the power spectrum and the underlying time series have statistically the same form on every scale and no scale is preferred. Power law power spectra are exhibited in many natural physical systems and are classified by their spectral exponent  $\alpha$ . In an isolated or autonomous system the value of  $\alpha$  can give clues as to the physical mechanisms by which they might be generated, such as Brownian motion or turbulence [e.g., *Schroeder*, 1991].

[7] However, in the coupled system of the solar wind-magnetosphere-ionosphere the situation is more complicated because the power spectrum of the solar wind driver itself is known to have a power law form [*Roberts and Goldstein*, 1991; *Burlaga*, 1995; *Goldstein and Roberts*, 1999]. At 1 AU, both the power spectrum of mainly incompressible waves measured by the trace of the interplanetary magnetic field (IMF) vector and of compressible waves measured by the magnitude of the magnetic field or velocity varies as  $f^{-5/3}$  for  $f > 0.03$  mHz (i.e., period less than  $\sim 1$  day).

[8] Thus the power law distribution of magnetopause reconnection timescales and power law power spectrum of associated ionospheric currents might not arise from some intrinsic property of the M-I system or reconnection process but instead reflect the spatial and temporal structure of the solar wind that drives reconnection. *Lockwood and Wild* [1993] showed that the probability distribution of inter-FTE intervals between 1 and  $\sim 30$  min was similar to the distribution of intervals between times when the north-south component  $B_z$  of the IMF was above or below the  $-2$  nT threshold. *Freeman et al.* [2000a, 2000b] examined similar properties of the solar wind Poynting flux and of the  $AU$  and  $AL$  indices that measure the peak strength of the eastward and westward auroral electrojets, respectively. All three quantities have power law probability distributions of durations for which the time series is above or below some fixed

**Table 1.** Summary of Previous Studies of Ground-Based Magnetometer Data and Ionospheric Electric Field Measurements Where Power Law-Like ( $f^{-\alpha}$ ) Power Spectra Have Been Found

Reference	Power Law Exponent, $\alpha$	Observation/Power Law Frequency Range, mHz	Data Interval	Magnetic Latitude
<i>Magnetic Field Measurements</i>				
<i>Campbell</i> [1976]	1.0–4.0	0.07–3.3	123 data years	79°S–89°N
<i>Consolini et al.</i> [1998]	2.6	0.4–6	2 months	77°S
<i>Francia et al.</i> [1995]	2.3–2.4 (daytime) 2.6–2.7 (nighttime)	>1.7	954 days	38°N
<i>Weatherwax et al.</i> [2000]	2.5	0.02–100	1 day	74°S 86.7°S 45°N
<i>Buchert et al.</i> [1999]	4.5	3–20	2.5 hours	66°N
<i>Electric Field Measurements</i>				
<i>Buchert et al.</i> [1999]	2	4–9	2.5 hours	66°N
<i>Bering et al.</i> [1995]	1.5	0.4–30	8 hours	74°S
<i>Weimer et al.</i> [1985]	1.8	0.001–0.1 km <sup>-1</sup>	2 passes	55–70° inv. lat

threshold, with the same power law exponent, independent of threshold, for durations between  $\sim 1$  and  $>100$  min. One interpretation of this observation was that fluctuations in the auroral DP2 currents are directly driven by fluctuations in the power input from the solar wind. *Tsurutani et al.* [1990] compared the power spectrum of  $B_s$  ( $B_s = \text{IMF } B_z$  when  $B_z < 0$ ,  $B_s = 0$  when  $B_z > 0$ ) with the power spectrum of contemporaneous AE index data that measures the total peak strength of the auroral electrojets. They found that the solar wind 5 min averaged data had a power law power spectrum over the observed range of  $0.01 < F < 1$  mHz with an exponent of  $\alpha \approx -1.4$ , similar to the turbulent spectrum noted above for the trace of the IMF vector in this frequency range. The AE 1 min averaged data had a similar power law power spectrum with  $\alpha \approx -1.0$  for  $f \leq 0.06$  mHz but a different power law power spectrum with  $\alpha \approx -2.4$  for  $f > 0.06$  mHz.

[9] A complication in the comparison of the temporal structure of solar wind and ground geomagnetic data has been raised by *Buchert et al.* [1999] who suggested that the exponent of a power law magnetic field power spectrum measured at the ground in the mHz frequency range is generally greater than that of the associated ionospheric current spectrum owing to the shielding of small-scale current structures from the ground. They observed a power law-like spectra with  $\alpha = -4.5$  for  $3 \leq F \leq 20$  mHz, when examining the  $X$  and  $Y$  components of the magnetic field measured by the IMAGE magnetometers at Tromsø and Kilpisjärvi from one 2.5 h sample on 18 October 1993 in the afternoon auroral zone. Simultaneous observations were made of the auroral electric field components and of the Hall and Pedersen conductivities at 278 km altitude in the F region ionosphere by the tristatic EISCAT UHF radar system that all showed evidence of a power law power spectrum component with  $\alpha \approx -2$ . The power law exponent of the ionospheric electric field is comparable with the  $\alpha \approx -1.4$ , turbulent-like spectrum seen at lower frequencies in the AE index magnetic field spectrum.

[10] Besides the *Buchert et al.* [1999] case study, we know of only two other studies that have measured the ionospheric electric field spectrum (see Table 1). Furthermore, we have found no other estimates in the literature of the power spectral exponent of the ionospheric electric field or  $\mathbf{E} \times \mathbf{B}$  velocity measured directly with radar in this frequency range (though similar work has been carried out using SuperDARN radar to look at the power spectrum of gravity waves, e.g., *Bristow and Greenwald* [1997]).

[11] In this paper we seek to advance our understanding of the spatiotemporal structuring of reconnection-driven ionospheric flows and currents by studying the power spectrum of ionospheric  $\mathbf{E} \times \mathbf{B}$  velocities measured with the SuperDARN CUTLASS Finland radar at the times of PIFs (as mentioned above, an ionospheric signature of reconnection). We also measure the power spectrum of contemporaneous magnetic field perturbations measured by nearby IMAGE magnetometers. The methodology and results are laid out in sections 2 and 3. In section 4 we discuss the assumptions and uncertainties associated with our analysis method and then compare and relate the ionospheric flow character to that of ground magnetic fluctuations. In section 5 we discuss a possible interpretation of these results in terms of multiscale reconnection at the

magnetopause driven by an intermittent, turbulent solar wind. Finally, in section 6 we summarize our results and conclusions.

## 2. Methodology

[12] This survey is based on velocity data from the CUTLASS Finland radar of the SuperDARN network [*Greenwald et al.*, 1995] and magnetic field data from the IMAGE magnetometer network [*Lühr et al.*, 1998].

### 2.1. Radar Power Spectra

#### 2.1.1. Radar Data Selection

[13] The SuperDARN radars measure backscatter from field-aligned ionospheric irregularities in the E and F regions. The radars transmit at fixed frequencies in the 8–20 MHz range and, from the return signals, estimates can be made of backscatter power, line of sight (LOS) velocity, and spectral width. The SuperDARN radars operate the majority of the time in common mode, in which the radar scans through 16 beams differing by  $3.25^\circ$  in azimuth. Nearly all data used in this survey have been collected using a transmitting frequency of 9 or 10 MHz and thus a beam width of  $\sim 5^\circ$ . In each beam 75 range gates are measured with a pulse length of 300  $\mu\text{s}$  (equivalent to 45 km) with a lag to the first range of 1200  $\mu\text{s}$  (equivalent to 180 km). During the 18-month interval under study the definition of common mode changed from 100 s for a complete scan across 16 beams to 120 s. The radars also operate in a variety of different modes which can have different time and/or spatial resolution.

[14] In order to reduce the work involved with data selection and in order that we might make a direct comparison we have used in this study the same PIF intervals as were used by *McWilliams et al.* [2000]. An example of one of these PIF intervals is provided by *McWilliams et al.*'s [2000] Figure 1. These PIF intervals cover the period March 1995 to September 1996, varied in length between 20 min and 7.5 hours, and included common mode and high time resolution radar data. In order to avoid any complications and inaccuracies involved with combining powers from different frequencies it was decided that any power spectra would be calculated from a time series of a standard length where the radar was operating in common mode resolution. Since the common mode resolution changed from 100 s to 120 s during the period under study, the length of time series chosen should be a multiple of both 100 s and 120 s.

[15] The choice of time series length used in this study has been made to balance a number of factors. First, the longer the time series the better the frequency resolution and range. Second, we desire a number of different time series, from different range gates, and from many intervals, so as to reduce the spectral uncertainty and to ensure our survey is not dominated by any one interval. Third, it is desirable to have complete time series with no data gaps, as interpolation across such gaps can introduce error into the spectra. Fourth, the entire time series must be contained in a PIF interval. The length of time series used must be shorter (or equal to) the length of the longest PIF interval (7.5 hours) but we will find few (if any) time series of this length, and any we do find will come from one interval. Using a time series length of 2 hours and not constraining time series

from the same interval to start at the same time, we obtain a total of 1294 time series from 58 of the 139 common mode intervals, with between 1 and 214 time series coming from any one interval. The data used come from between  $69^\circ$  and  $87^\circ$  AACGM latitude and 0415–2230 MLT. While the range of MLT included in this survey is very large, extending well away from noon, 75% of time series are taken between 0800 and 1600 MLT with a peak around 1000 MLT. Our range of MLT is larger than that of *Provan and Yeoman* [1999] who observed PIFs from 0250 to 1650 MLT with the CUTLASS Finland radar (also with a peak around 1000 MLT). This is probably due to our inclusion of all suitable time series within the radar field of view at the time of PIFs. The location and distribution of scatter used is shown in Figure 2.

[16] Unwanted ground scatter was removed by rejecting those data which have LOS velocities  $<30 \text{ m s}^{-1}$  and spectral widths  $<35 \text{ m s}^{-1}$ . Many other ground scatter data have also been ignored owing to our stringent criteria for the selection of time series which must have no data gaps, as misidentified ground scatter is most often seen embedded within regions of correctly identified ground scatter. However, it is inevitable that some ground scatter has been included in this survey. A more complete removal of ground scatter from the data set could be achieved [Chisham and Pinnock, 2002] by increasing the limits set for the identification of ground scatter from those used; however this would also lead to the unwanted removal of real ionospheric scatter. This would lead to fewer time series available for use (in fact considerably so) with a consequent increase in spectral uncertainty. Also, those time series which were used would contain a bias insofar as they would include time series with a disproportionate amount of larger jumps from positive to negative flow velocities, the effect of which is not immediately obvious.

[17] We have not discriminated between radar data other than to restrict it to times when PIFs are in the FOV. Our criteria for 2 hours of continuous data has further restricted the data we are using to the main body of scatter rather than the on-off scatter of the PIFs themselves. The majority of the scatter we have used is located in the cusp region, though we have undoubtedly included data from equatorward of the high/low spectral width boundary (which is often used as a proxy for the open/closed field line boundary).

[18] It is possible that solar wind conditions may also have a bearing on the power spectra we observe. While the original survey of *McWilliams et al.* [2000] was biased toward intervals of southward IMF (67% of times  $B_z < 0$ ) this is not the case for the subset of intervals used here. By imposing our stringent requirements that 2 hours of continuous radar data were required in any particular time series, we have unintentionally imposed a different bias on our events. Since the cusp is a good target for HF radar backscatter, we have favored those times when the cusp remains in the radar field of view (FOV) as there is then an increased likelihood of continuous observations for over 2 hours. This, in turn, means that we have biased ourselves toward times when the IMF  $B_z$  is either continually changing between positive and negative or weakly positive such that the cusp does not significantly change latitude. This also explains why the majority of scatter we have used

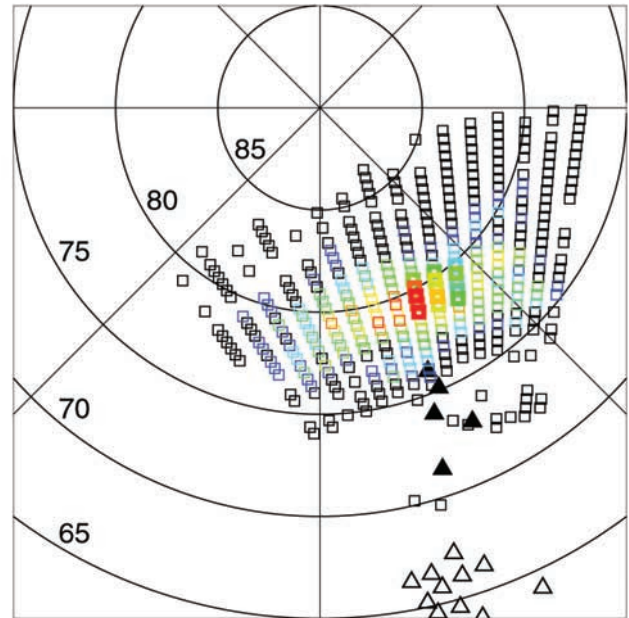


**Figure 2.** The location of radar scatter and magnetometers used in this study plotted in AACGM coordinates with an assumed height of 300km for the radar scatter. The circles indicate lines of geomagnetic latitude every  $5^\circ$ . Lines of geomagnetic longitude are plotted every  $45^\circ$  with  $0^\circ$  located at the left of the plot. The colored squares indicate the approximate location of the range-gate from which radar scatter was used in this study. The color indicates how many time series were used from each range-gate (black = 1, red = 10). The 15 bold squares indicate the group of cells used in the spatial averaging simulation in section 4. The black triangles indicate the positions of the IMAGE magnetometers. Only the five northernmost Svalbard magnetometers were used (filled triangles).

occurs at higher geomagnetic latitudes than would normally be associated with the cusp.

### 2.1.2. Calculating Individual Radar Power Spectra

[19] The method employed for calculating individual power spectra for each of the 1294 2-hour time series is as follows: (1) Subtract a linear least squares fit of the time series from the time series. (2) Apply a Hanning window  $[\cos(2\pi i/(n-1))]/2$  to the time series. (3) Subtract the mean value of the time series from the time series. (4) Perform an FFT on the time series. (5) Multiply each element by its complex conjugate. (6) Extract positive frequency values. (7) Double the value in all but the highest frequency bin. (8) Normalize the time series to the total power (variance-normalization).

### 2.1.3. Combining Individual Radar Power Spectra

[20] A single power spectrum representing all the 1294 2-hour individual power spectra was derived by finding the median and upper and lower quartiles of all 1294 PSDs at each frequency. Percentiles were used in order that extreme values did not affect the combined spectrum. Nevertheless, this method may tend to give a bias toward intervals with many time series (range gates) available. To ensure that such biases were not affecting the results, we also employed a different method in which the median of the variance-

normalized power spectra for all time series in each interval was calculated, and then the median of such spectra over all intervals was derived. This may tend to bias those events with few time series available. As will be shown later, the difference in the spectra obtained from each method is minimal.

## 2.2. Magnetometer Power Spectra

### 2.2.1. Magnetometer Data Selection

[21] We have used 10 s magnetometer data from the IMAGE magnetometer network which lies beneath the Finland radar FOV. Figure 2 shows the location of the IMAGE magnetometers relative to the location of radar scatter used. Most of the scatter used lies poleward of the IMAGE magnetometers and so is not ideal for a direct comparison. In most cases the IMAGE magnetometers will be located equatorward of the open/closed field line boundary. Some preliminary work (not shown), using all the IMAGE magnetometers, indicates that there are systematic differences in the spectra of the ionospheric currents at different magnetic latitudes. The change in power law exponent with latitude is not simple and certainly not linear and may contribute to the difference we see between radar and magnetometer spectra described below. While most of the IMAGE magnetometers are well equatorward of the scatter, the five magnetometers on the Svalbard archipelago lie within some of the scatter region and within  $3\text{--}8^\circ$  of the peak backscatter region. These are indicated in Figure 2 by the solid triangles and are the magnetometers that were used in this survey. In order to reduce data retrieval we have only used the five PIF intervals which produced the highest number of continuous 2-hour time series. These intervals gave rise to 58 continuous 2-hour time series from the five magnetometers used.

### 2.2.2. Calculating Magnetometer Power Spectra

[22] To make as direct a comparison between the power spectrum of the flows and magnetic field fluctuations as possible, we have mimicked the radar data collection by using one 10 s magnetic field values sampled every 2 min. While the IMAGE data set does not show any data gaps, a closer inspection reveals that there are some short intervals which have been interpolated across. However, these data are not evident in the sampled data and we have not accounted for them in our method. We have then computed the individual power spectra and median power spectrum of all three components of the magnetic field using the identical methods outlined above for the radar velocity data.

## 3. Results

[23] Figure 3 shows examples of radar power spectra from six different intervals. Figures 3a and 3b show the power spectra from two intervals from which only one range gate had an uninterrupted 2-hour time series that satisfied our criteria. We see a general decrease in PSD from low to high frequencies, though in each spectra there are a number of frequencies which have significant power associated with them and others with very little power, giving the impression of a highly structured spectra. Figures 3c and 3d show power spectra from two intervals which each produced 10 suitable time series. In this case the solid line shows the median of the 10 variance-normalized power spectra, and the dotted lines show the upper and lower quartiles. Again we see a general

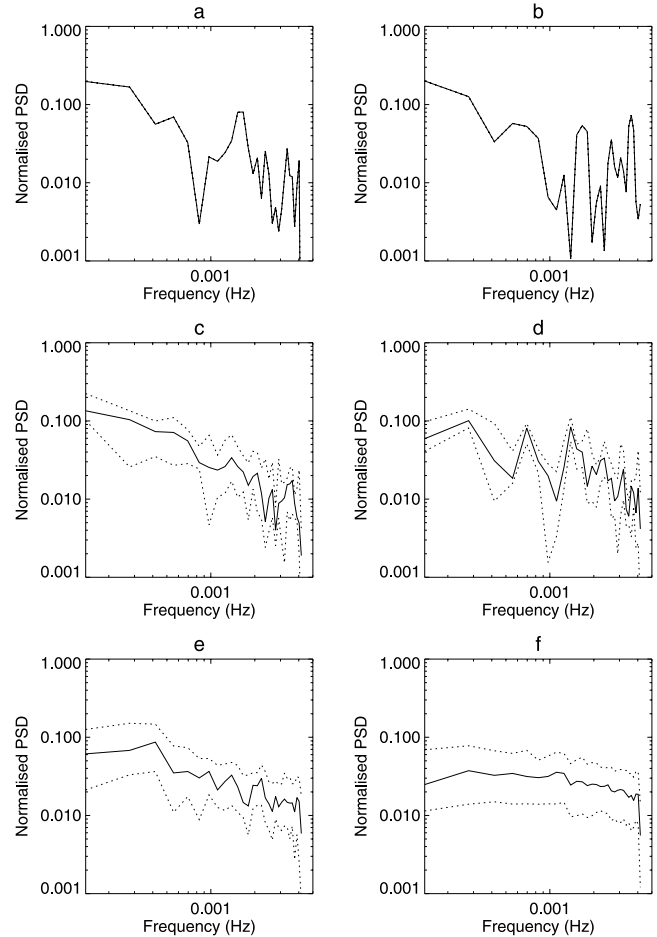


**Figure 3.** Examples of power spectra of individual PIF intervals. The solid line shows the median variance-normalized PSD and the dashed lines (where present) shows the upper and lower quartiles. (a) and (b) The power spectra from PIF intervals where only one time series satisfied our selection criteria. (c) and (d) The power spectra from PIF intervals where ten time series satisfied our selection criteria. The power spectra in Figures 3e and 3f were calculated from PIF intervals which provided 40 and 214 time series, respectively.

trend of decreasing power from low to high frequencies. While there is still some structure evident in the spectra there is far less than in Figures 3a and 3b. Figure 3e shows the median spectra from an interval which produced 40 time series and Figure 3f shows the median spectra from the interval which produced the most time series (214). We see that as we combine more spectra together, the structure diminishes though the general trend remains. By the time that the number of time series combined is 214 there is very little structure left in the power spectrum.

[24] Figure 4 shows the median power spectrum for the entire radar survey combined, using the two methods described in section 2.1.3. Figure 4a shows the result of simply taking the median variance-normalized PSD of all time series, while Figure 4b shows the result of taking the median variance-normalized PSD over each interval first and then combining all the intervals. The resulting power spectrum is power law-like. The straight line drawn on each

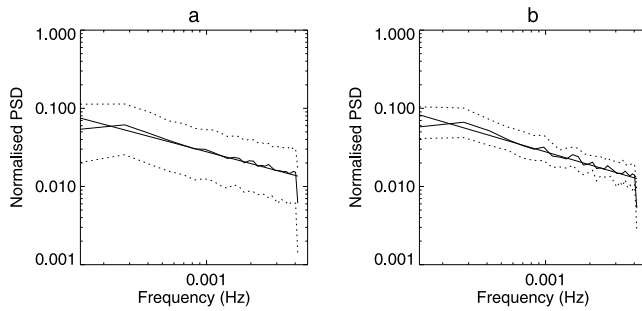


**Figure 4.** The median variance-normalized LOS velocity power spectrum for all 58 PIF intervals. The solid line shows the median PSD and the dashed line shows the upper and lower quartiles. On each plot a straight line is plotted which has been fitted to all 30 points. (a) The results of taking the median over all time series. (b) The result of taking the median over each interval first and then over all intervals.

log-log plot is a least squares fit to all 30 points. The slope of the line is  $-0.50 \pm 0.04$  in Figure 4a and  $-0.55 \pm 0.04$  in Figure 4b. Clearly, the two methods of combining power spectra produce very similar results. Almost no structure is seen in either power spectra and the slopes are almost identical. The difference between the upper and lower quartile traces in the two plots is simply due to the fact that in Figure 4b the variation is reduced owing to the fact that the spectra represents the median of 58 intervals rather than 1294 time series. In both Figures 4a and 4b the PSD at the lowest and highest frequencies is significantly less than the power law suggested by the other points. The lack of measured power at the highest frequency can be understood as this is the Nyquist frequency and must be considered a lower limit to the power at that frequency (owing to a lack of phase information). The lack of power at the lowest frequency can be understood as the effect of using a Hanning window, which spreads power into the DC component, which is then set to zero by subtracting the mean.

[25] Figure 5 shows the median power spectrum for each magnetic field component for the entire magnetometer survey, combined by taking the median of the power spectra from all time series. As with the radar data, there was very little difference between the spectra using the two combining methods (not shown). There is more structure in the magnetometer spectra than in the radar spectra which is simply due to the fact that only 58 time series have been used in the construction of the power spectra for each component of the magnetic field compared with 1294 time series used in the radar study. As with the radar data, the magnetic field spectra are power law-like and display some evidence of a roll-off at the lowest frequencies. The slopes of the best fit straight lines to all 30 points are  $-1.3 \pm 0.1$  for  $B_x$  (Figure 5a),  $-1.1 \pm 0.1$  for  $B_y$  (Figure 5b), and  $-1.3 \pm 0.1$  for  $B_z$  (Figure 5c).

## 4. Interpretation

### 4.1. Effect of Viewing Direction

[26] The results of the radar survey presented here are based on velocity measurements along different LOS. The angle between the LOS and geomagnetic north varies with

radar beam and range, and the angle between the LOS and the mean flow direction varies also with time owing to the Earth's rotation under the global-scale convection pattern. In combining the LOS velocity spectra from different beams and ranges and from different intervals with different global convection patterns, it is assumed that these spectra are independent of the LOS. Support for this assumption is provided by the similarity of the power spectra of the components of the measured magnetic field perturbations. Thus we would anticipate that the same should be true for the ionospheric velocity.

### 4.2. Effect of Earth's Rotation

[27] The radar location and LOS changes relative to the global convection pattern over the course of our 2-hour time series owing to the Earth's rotation. To examine what effect this may have, we consider the case where all temporal variations arise owing to the propagation of a spatially structured field over an observer. The frequency,  $\omega$ , in a field at rest with regard to the global convection system is related to the wave vector,  $\mathbf{k}$ , and propagation velocity,  $\mathbf{v}$ , by

$$\omega = \mathbf{k} \cdot \mathbf{v}. \quad (1)$$

In the frame of the Earth (our observing frame) the propagation velocity  $\mathbf{v}'$  is  $\mathbf{v} + \mathbf{a}$ , where  $\mathbf{a}$  is the velocity of the Earth's surface. The observed frequency,  $\omega'$ , is thus given by

$$\omega' = \omega \left( 1 + \frac{\mathbf{k} \cdot \mathbf{a}}{\mathbf{k} \cdot \mathbf{v}} \right). \quad (2)$$

Given that MHD fast and Alfvén wave speeds in the magnetosphere correspond to propagation speeds of order  $10^4 \text{ m s}^{-1}$  in the ionosphere and the speed of the Earth's

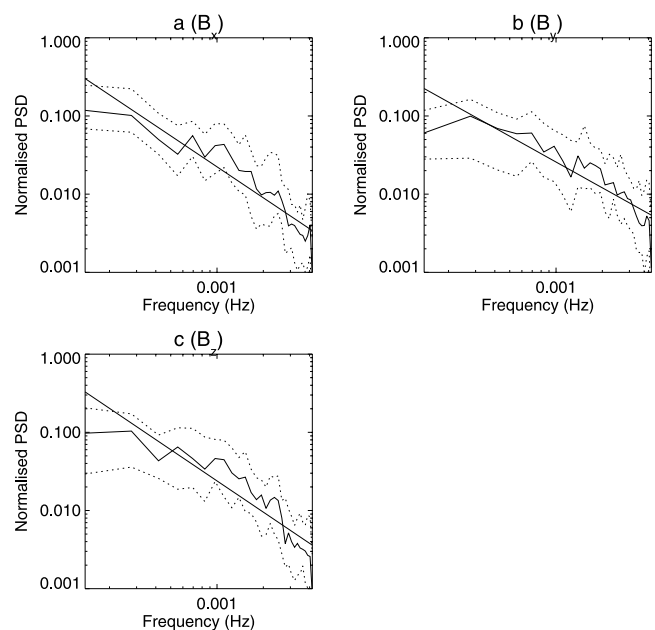


**Figure 5.** The median variance-normalized magnetic field power spectrum for the five dominant PIF intervals. The format of each panel is the same as Figure 4a.

surface at  $79^\circ$  latitude,  $89 \text{ m s}^{-1}$  eastward, normally  $\mathbf{k} \cdot \mathbf{a} \gg \mathbf{k} \cdot \mathbf{v}$  and thus  $\omega' \approx \omega$ . Generally, the effect of the Earth's rotation will be small, and we can attribute the measured spectra purely to the temporal variations in the flow.

### 4.3. Correction to Power Law Exponent

[28] The discrete Fourier transform of a finite sample of a longer parent time series can provide only an estimate of its power spectrum. A better estimate can be obtained by combining many samples together. However, even so, using a time series of finite length will add leakage into the estimated spectrum. Using windowing functions (such as the Hanning window we have applied here) reduces leakage but instead introduces spread into the signal. Both the introduction of spread and leakage into a power law-like spectrum will act so as to decrease the slope of a power law. Qualitatively, we can understand this in terms of power in each frequency bin being spread equally between bins at lower and higher frequencies that results in a net transfer of power from frequencies with higher PSD to those with lower PSD (rather akin to a diffusion process).

[29] In order to place a meaningful interpretation on our result, we need to understand the quantitative effect of our windowing function on the measured power law exponent. To investigate this, we have attempted to reproduce the effect by simulation. Ideally, we would like to sample an infinite, continuous parent time series with a power law power spectrum in exactly the same way as the real data. Practically, we can only create a parent time series with a finite time step  $\Delta t$  and of finite length  $m\delta t$ . What we then require is for this parent time series to (1) have a time step  $\Delta t$  that is small compared with the time step  $\Delta T$  of the sampled time series (i.e.,  $\Delta T/\Delta t = n_1 \gg 1$ ) and (2) be long compared with the  $M$ -point sampled time series (i.e.,  $m\Delta t/M\Delta T = n_2 \gg 1$ ). Using  $M = 60$  (i.e., 2-h sample at 2-min resolution), the number of points in our parent time series will then be  $60n_1n_2$ . In the simulation results presented below, we have used  $2^{20}$  (1048576) points in the parent time series, i.e.,  $n_2 \approx n_1 = 132$ . Consistent results have been achieved by repeating the analysis outlined below with  $2^{19}$  points (i.e.  $n_2 \approx n_1 = 93$ ), indicating the number of points in the parent time series is sufficient.

[30] We build up a 60-point time series,  $v(t_j)$ , for times  $t_j = n_1 j \Delta t$  where  $j = 0, 1, 2, \dots, 59$ , by summing  $2^{19}$  frequency components (corresponding to a full spectrum with positive and negative frequencies of  $2^{20}$  points) with random phase, i.e.,

$$v(t_j) = \sum_{i=0}^{2^{19}} A_i \sin(2\pi i t_j + \phi_{ri}), \quad (3)$$

where  $A_i^2 = i^{-\alpha}$ , and  $\phi_{ri}$  is a random phase element for each of the  $2^{19}$  frequency components uniformly distributed between 0 and  $2\pi$ . The resultant time series is equivalent to sampling the  $2^{20}$  point time series every  $n_1$  points. The power spectrum of this 60-point time series was then calculated using the same method we have employed for the radar and magnetometer data.

[31] For a particular value of  $\alpha$ , the simulation was run 200 times. For each power spectrum a straight line was fitted in log-log space. The mean and standard deviation of the slopes of these straight lines were then recorded. This

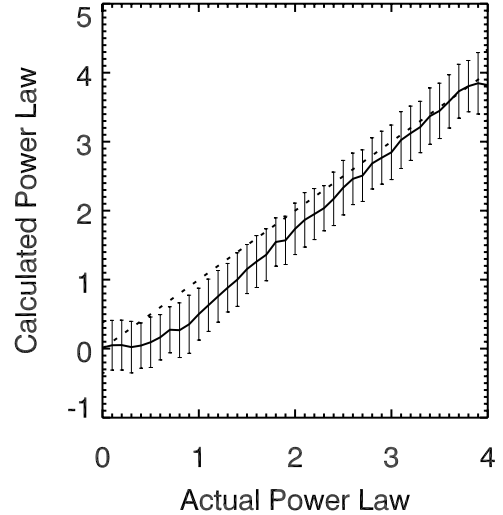


**Figure 6.** The simulated variation between the actual power law and the power law calculated using our employed method. The error bars show  $1\sigma$ .

process was repeated for 40 different values of  $\alpha$  between 0 and 4. The results of the simulations are shown in Figure 6. It can be seen from Figure 6 that the estimated power law slope is in fact less than that of the actual slope, especially at the lowest values of  $\alpha$ . We have repeated this analysis using both no windowing function (which can be thought of as a square window) and using the Hanning window applied to the autocorrelation function (results not shown) but both prove less satisfactory than the results shown in Figure 6. We can use Figure 6 as a diagnostic tool to relate the calculated slope of the radar and magnetometer power spectra to an actual slope once we assume that the power spectra are indeed power law spectra. We find that the measured slope found in the radar survey of  $-0.5$  corresponds to an actual slope of  $-0.9 \pm 0.3$  and that the measured slope found in the magnetometer survey of  $-1.3$  corresponds to an actual slope of  $-1.8 \pm 0.3$ .

### 4.4. Variability of PSD Introduced by Using Finite Time Series

[32] The above argument holds only if it is true that the measured finite time series are in fact part of a longer time series which is power law-like. It is possible to imagine a situation where a large number of power spectra containing only a few narrow individual peaks could average out to a power law, but one would not say that the individual time series were representative of a power law distribution. The fact that the spread in the fitted slope is the same in the simulation and in the data gives us some confidence that this is not the case. We have also investigated the structure in the individual power spectra.

[33] We have defined a spikiness index as being the mean absolute deviation of the  $\log_{10}$  of the PSD from the straight line fit. Figure 7 compares the distribution of spikiness from our radar survey (solid line histogram) with that from our simulation with a power law slope of  $-0.95$  (dashed line). We can see that the two curves agree very well. We thus interpret the structure seen in the spectra of individual radar velocity time series (Figures 3a and 3b) as arising from

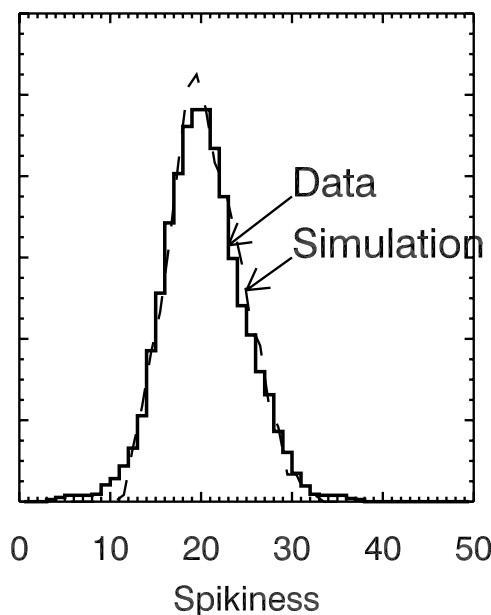


**Figure 7.** The comparison between the distribution of spikiness of a power spectrum between our observations made with the radar (solid histogram) and a simulated power law time series (dashed line) with an exponent of 0.95.

using short intervals taken from an infinite time series with a power law-like spectrum of exponent  $\approx 1$ . Similarly, the curves in Figure 8 compare the distribution of spikiness from our magnetometer survey (solid line histogram) with that from our simulation using a power law slope of  $-1.6$  (dashed line). The distributions do not agree so well.

#### 4.5. Relationship Between Radar and Magnetometer Spectra

[34] One immediate question which needs to be addressed is why we see such different power spectra between the magnetic fields and the ionospheric flows (currents) which are giving rise to them. Previously, *Buchert et al.* [1999] found similar differences between the power spectra of magnetometer data and electric field and conductivity measurements made with the EISCAT incoherent scatter radar. They suggested that these differences were due to the magnetometer being influenced by ionospheric currents flowing over a large area (of the order of a few hundred kilometers square), while the EISCAT radar measurements were taken from a much smaller ionospheric area (of the order of a few kilometers square). Effectively, what is happening is that the magnetometers are spatially averaging over the ionospheric current system.

[35] With the SuperDARN radar we have the ability to test this hypothesis because we have measurements of the ionospheric flows across a spatial FOV. For the common mode measurements used here, a 3-beam by 5-range gate area is  $\sim 300$  km square and roughly corresponds to the area over which a magnetometer is influenced by currents. Thus we attempted to find a fixed 3-beam by 5-range gate area which, for each magnetometer interval, had continuous data for 2 hours, starting simultaneously, for 10 of the 15 range gate cells. In this way, we could keep the method of

estimating the PSD identical to that which we have used for the rest of the study, and the data used would also be taken from the PIF intervals which have been used in the magnetometer survey, so as to aid a direct comparison. In reality this proved impossible, but we were able to satisfy the above criteria for 4 of the magnetometer intervals and one other PIF interval. The 3-beam by 5-range gate area used is indicated in Figure 2 by the bold squares.

[36] For each time step we then averaged the LOS velocities from the 10 continuous time series to roughly mimic the magnetometer measurements. The power spectrum was then calculated for each interval using the identical method as described above. As before, the power spectra for each interval were variance-normalized and the median power spectrum was found by taking the median of each frequency bin (note the two averaging methods are now identical as we only have one time series for each interval). The spatially averaged power spectrum is shown in Figure 9.

[37] There is a large amount of variation in the power spectrum shown in Figure 9 compared with the corresponding magnetometer power spectra (Figure 5). This is simply due to the fact that only five time series have been used in the spatially averaged LOS velocity survey compared with 58 in the magnetometer survey. Nevertheless, we can see a clear increase in slope compared with that of the original LOS velocity spectrum (Figure 4). Fitting a straight line to all 30 points provides a power law slope of  $-0.9$ . There is evidence that by ignoring the lowest 4 or 5 frequency bins a steeper slope would be found, though due to the nature of the fluctuations seen in the power spectrum there is little justification for doing this.

[38] The effect of spatial averaging to steepen the power spectral slope can be understood by considering the likely

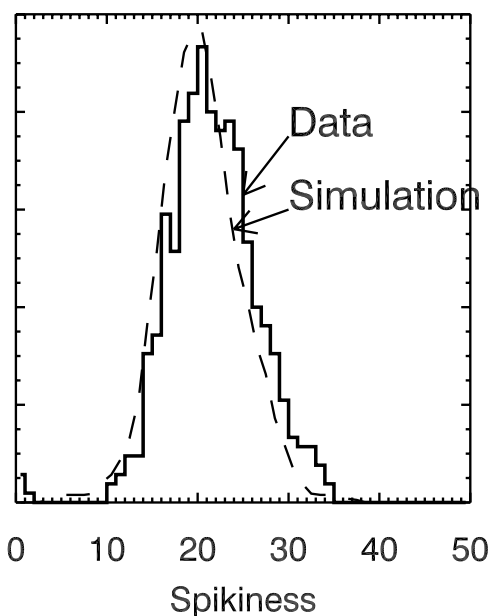


**Figure 8.** The comparison between the distribution of spikiness of a power spectrum between our observations made with the magnetometer (solid histogram) and a simulated power law time series (dashed line) with an exponent of 1.8.

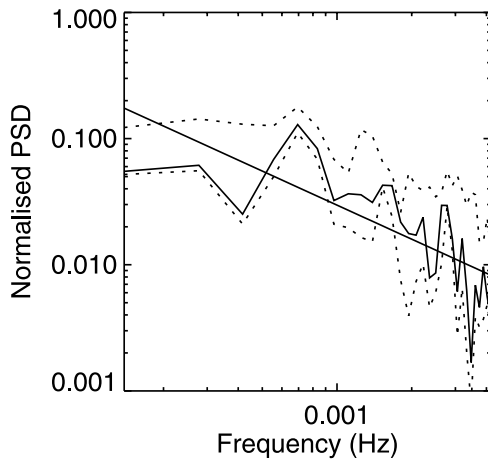


**Figure 9.** Variance-normalized median power spectrum of spatially averaged LOS velocities. The format of the plot is the same as Figure 4a.

relationship between the spatial and temporal structure. We would expect long spatial variations to be related to long period (low-frequency) temporal variations and vice versa. Another way of considering this is that on any particular spatial scale we would expect lower-frequency oscillations to be more in phase than higher-frequency oscillations. Averaging  $n$  Fourier components of the same frequency  $f$ , differing amplitudes  $A_i$ , and the same phase  $\phi$  will produce a signal with the average amplitude of the components. In contrast, averaging the same Fourier components with random phase will in general produce a signal at the same frequency  $f$  with a smaller amplitude (generally, this will be non-zero except in the special case where all components cancel exactly). In fact, the expected value of the amplitude will go as  $n^{-1/2}$  and the power will go as  $n^{-1}$  (as  $n \rightarrow \infty$ , power  $\rightarrow 0$ ). In between these two extremes, the average power will vary such that averaging signals which are more in phase will result in more power than averaging signals which are less in phase. Following this argument, it is easy to see how averaging a number of time series with a power law-like power spectrum where the low-frequency variations are more in phase than the high frequencies will lead to a steepening of the spectral slope.

[39] Figure 10a shows the variation of the spatial variability of phase with frequency for the radar data used in the spatially averaged power spectrum of Figure 9. The phase of each frequency component was calculated using the same Fourier transform techniques as we have used to calculate the power spectra. For each interval and each frequency bin we have calculated the standard deviation of the phases from the 10 grouped range gate time series (after adding  $2\pi$  to any relevant phase values such that the spread was minimized). What is plotted in Figure 10a is the mean of these values over the five intervals for each frequency bin. We have not employed a more familiar coherence function type analysis, as this would not take account of any systematic phase offset between two range-gates (i.e. two time series can have a coherence of one while having different phases). What can clearly be seen in Figure 10a is an increasing spread in phase between the lowest frequencies and 1 mHz. Above 1 mHz the plotted quantity saturates.

One should not attach a great significance to this frequency, as it is a function of the number of points used in the calculation. The saturation arises as a result of the necessity of measuring the standard deviation of the phase such that the spread is minimized that consistently underestimates the value for a random sample of phases.

[40] We have been able to reproduce the behavior seen in Figure 10a using the same type of simulation as used in section 4.4. In this simulation we used an original power law exponent of  $\alpha = 0.95$  which corresponded to the measured exponent of  $\alpha = 0.5$  found in Figure 4. We create 10 time series in the same way as in the previous simulation except this time there are two random elements to the phase. As before, each frequency component has a random phase, though they are identical across the 10 time series. A further normally distributed random phase is applied to each frequency component, which is different for the 10 time series. The standard deviation of the normal distribution  $\sigma_R$  varies with frequency bin  $i$  ( $i = 1, 2, \dots$ ) such that  $\sigma_R = (1.2 \times 10^{-4}i) + 0.28$ . We have then taken the mean of the ten 60-point time series (similarly to our spatially averaged power spectra) and calculated the Fourier transform in the same way. Again this was repeated 200 times. Figure 10b shows the results of the phase spread analysis used in Figure 10a applied to the simulated data. Apart from the smoothness of the data (due to a sample of 200 points compared with 5) the results are very similar. Also, the mean slope measured in the simulated power spectra is  $-0.8$  which again is very similar to the measured spatially averaged spectral slope of  $-0.9$ . It should be noted that by using the additional random phase component we do not address any systematic spatial phase differences which may occur given that there is likely to be a preferred propagation direction. However, this will still give rise to a similar variation of phase variability with frequency.

[41] In summary, we have provided evidence that the spatial averaging effect of the magnetometers increases the spectral slope in the same sense as to explain the differences between the radar and magnetometer survey. We suggest that the spectral steepening is due to multiscale spatial structure that gives rise to a phase difference between nearby locations which varies with frequency. We have shown that such a phase relation exists in the radar data and reproduced the spectral-steepening effect in simulation, although our simplistic approach has not increased the spectral slope to the same value as in the measured

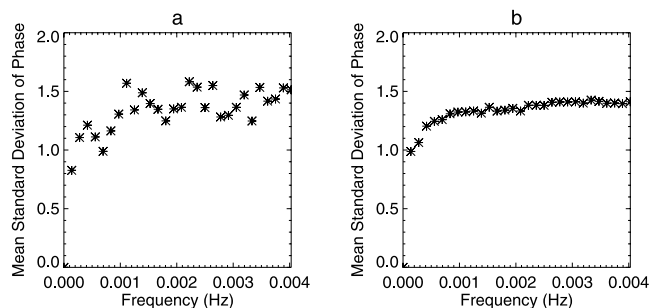


**Figure 10.** The mean standard deviation of phase of Fourier components as a function of frequency averaged over (a) the five intervals of radar data used in Figure 9 and (b) 200 intervals of simulated data.

magnetometer spectra. It is worth noting that simply by increasing the number of time series we average over a further steepening of the spectral slope will be achieved and that other factors such as conductivity may come into play.

[42] One might argue that if the power law slope has been steepened in the magnetometer survey by spatial averaging, how can we be sure that the same has not happened in the radar survey. It may be that on the spatial scale of the radar measurements all frequencies of interest are fully in phase and so there will be no change to the spectral slope owing to spatial averaging. Each radar cell has a dimension of 45 km along the beam and a variable dimension across the beam depending on the range of the measurement. This beam dimension varies between 106 and 290 km for the data used here, though 75% of measurements have dimensions between 185 and 235 km. While it is possible that spatial variations responsible for the temporal frequencies of interest are in phase across the 45 km range dimension, there is certainly going to be some spatial averaging effect due to the beam width. However, the area sampled by each radar cell is considerably less than that influenced by the magnetometers and so any effect will be considerably smaller. It is possible that the spatial averaging has an effect on the spikiness index defined in section 4.4. The deviation of the data spikiness distribution from the simulated distribution in Figure 8 could be due to the spatial averaging effect, in which case there would appear to be little spatial averaging affecting the radar distribution. In reality, spatial averaging is expected to cause a steeper spectral slope of the radar survey to some degree, and so we must treat our estimated values of  $\alpha$  as an upper limit.

## 5. Discussion

### 5.1. What Does a Power Law Power Spectrum Mean?

[43] We have shown here that the ionospheric flows and associated magnetic field perturbations found in the cusp are power law-like and exhibit self similar behavior, i.e., there are no preferred frequencies. This may initially appear to be inconsistent with many observations in this region where distinct frequencies have been seen. However, it is not. We have shown that spectra from individual time series can and do display enhanced power at a limited number of frequencies but that this is entirely consistent with studying finite intervals of an infinite time series with a power law spectrum. This should not be taken to mean that these signals are not real, rather that any one time series is not a representation of the overall population. Thus one must also be careful in looking for a particular signal, indicative of a physical process with a definite timescale. By trawling through much data with scale-free character, many examples of short time series with enhanced power at a given frequency can be found. All of this is not to say that processes with distinct timescales do not exist, rather that they do not appear significant within our sample.

### 5.2. Comparison With Previous Studies

[44] As discussed in section 1, there have been previous studies which have found a power law-like power spectrum in measurements of electric and magnetic fields. The main difference between our results and those summarized in Table 1 is the value of the spectral exponent. The spectral

exponent of 0.9 that we suggest describes the radar data in this survey is less than the values of *Buchert et al.* [1999], *Bering et al.* [1995], and *Weimer et al.* [1985] of between 1.5 and 2. These differences can be explained by examining the method and interpretation employed in each study.

[45] *Buchert et al.* [1999] used a single 2.5 hour time series in calculating the electric field power spectra. Moreover, the power law-like part of this spectra only covers the frequency range 4–9 mHz. Examination of *Buchert et al.*'s [1999], Plates 4 and 5 show that there is considerable structure and variation in the power spectra and that there must have been a large uncertainty in the determination of the power law exponent of 2. In the case of *Bering et al.* [1995] the electric field was measured directly using double probe electric field detectors mounted on a balloon flying at 32 km altitude. In their discussion they note that the magnetospheric electric field is screened by the ionosphere at altitudes of 30 km and that this screening is greater for large-scale perturbations than small-scale perturbations. This will tend to steepen the spectral slope in much the same way as the spatial averaging effect of the magnetometers described in section 4.5 (though not necessarily to the same extent). This steepening may explain the difference between the *Bering et al.* [1995] spectrum and the spectra presented here. *Weimer et al.* [1985] inverted the electric field time series measured with the DE-1 and DE-2 spacecraft and presented a spatial frequency spectrum rather than a time frequency spectrum. Thus the measured power law exponent is not directly comparable to the power law exponent estimated in this study. It is worth noting that the methodology of *Weimer et al.* [1985] assumes a steady state electric field, which we have demonstrated is not the case. However, their study does support our suggestion that there is spatial structure at a number of scales.

[46] Our suggested magnetic field power law exponent of 1.8 is within the range of 1.0–4.0 found by *Campbell* [1976] though somewhat smaller than the other studies listed in Table 1. With the exception of the *Buchert et al.* [1999] study, all the listed studies use reasonable amounts of data and there are no particular aspects of their methodology which would give us reason to expect different exponents. We suggest rather that observations made in different geophysical regions may have different spectral exponents. However, note that while *Francia et al.* [1995] did find different power law exponents on the dayside and nightside, *Weatherwax et al.* [2000] found the power law exponent to be unchanged over a wide range of latitudes, and indeed between very different solar wind conditions.

### 5.3. A Possible Physical Interpretation of the Power Law Power Spectrum

[47] In section 1, with reference to Figure 1, we discussed how both observations of magnetopause FTEs and of FTE-associated ionospheric phenomena, such as PIFs, display possible evidence of self-similar behavior. Given that we have also found evidence of self-similar behavior in PIF-associated ionospheric velocity and magnetic field fluctuations and that FTEs are generally considered signatures of time varying reconnection at the dayside magnetopause, we examine our results in the context of an open magnetosphere. We consider a simple electrical circuit

model of the open magnetosphere and how the time variation of the solar wind may be reflected in the ionosphere through reconnection.

[48] *Sanchez et al.* [1991] modeled the tailward convecting part of the open magnetospheric system using a simple LR circuit based on the formalism of *Holzer and Reid* [1975]. In this model the magnetospheric segment of the circuit runs along the full length of the boundary associated with tailward flux transport, dropping down field lines at each end to the ionosphere, across which it closes. The resistance (R) of the circuit is provided by the ionosphere, and the inductance (L) is a combination of self-inductance and inductive inertia. The voltage source of the circuit is the full transpolar voltage. *Sanchez et al.* [1991] suggested that the PSD of the transpolar magnetopause voltage ( $P_{EMF}$ ) could be related to the PSD of the transpolar ionospheric voltage ( $P_F$ ) by

$$P_F = P_{EMF}(f)(1 + f^2\tau_{RL}^2)^{-1}, \quad (4)$$

where  $\tau_{RL}$  is the inductive response time of the circuit. Given that the solar wind input to the magnetospheric system (e.g.,  $vB_s$  and  $\epsilon$ ) is temporally scale-free over the timescales we have studied in the radar data [e.g., *Tsurutani et al.*, 1990; *Freeman et al.*, 2000a, 2000b], we can assume  $P_{EMF} = Af^{-\alpha}$ . We then find

$$P_F = A(f^\alpha + f^{\alpha+2}\tau_{RL}^2)^{-1}. \quad (5)$$

This suggests that one would expect  $P_F$  to follow  $f^{-\alpha}$  when  $f \ll \tau_{RL}^{-1}$  and  $f^{-(\alpha+2)}$  when  $f \gg \tau_{RL}^{-1}$ . *Sanchez et al.* [1991] suggest a conservative value for  $\tau_{RL}$  of 20 min, though it may be as low as 4 min. This is within the frequency range we have measured for the ionospheric flows, but we do not see any such change in the PSD of the ionospheric voltage reflected in our velocity spectra. Furthermore, given that the measured exponent of  $B_s$  is  $-1.42$  [*Tsurutani et al.*, 1990], we would expect to see power law slopes  $>3$  in our radar studies above  $\tau_{RL}$ . Assuming the ionospheric velocity PSD reflects that of the ionospheric voltage, our results are inconsistent with the model we have described here unless  $\tau_{RL} > 1$  hour. (Note that such a break has been observed in the PSD of the AE index at  $f = \frac{1}{5}$  hour $^{-1}$  [*Tsurutani et al.*, 1990] but is attributable to the characteristic substorm timescale [*Takalo and Timonen*, 1994; *Watkins*, 2002]).

[49] What may be a more realistic solution is to model the reconnection circuit not as a single circuit with a single response time but as many circuits with a range of response times. (It is possible to form a  $f^{-1}$  like power spectra by combining a number of relaxation processes with different timescales [*Schroeder*, 1991]). This idea seems plausible if one considers the turbulent nature of the solar wind and that consequently reconnection may be initiated in patches across the dayside magnetopause with a range of sizes each with their own  $\tau_{RL}$  timescale.

## 6. Summary and Conclusions

- The median variance-normalized power spectrum of LOS velocity at the time of PIFs are power law-like, with a

slope of  $-0.50 \pm 0.04$ , which corresponds to an actual slope of  $-0.9 \pm 0.3$ , as expected in some long-range correlated systems.

- The median variance-normalized power spectrum of magnetometer data during same intervals are power law-like, with a slope of  $-1.3 \pm 0.1$  for the x and z components and  $-1.1 \pm 0.1$  for the y component. These correspond to an actual slope of  $\simeq -1.8 \pm 0.3$ .

- The difference between the radar LOS velocity spectra and the magnetic field spectra can, at least in part, be explained by the spatial averaging effect of a spatially structured field by the magnetometer.

- We have shown that much care must be taken in the interpretation of power spectra, both in terms of the slope of a power law-like spectrum and in terms of the apparent structure observed in a short time series.

- The spectral slope of the ionospheric velocity spectrum and the variability seen in individual ionospheric velocity power spectra are consistent with a single scale-free process. It is proposed that this scale-free nature may arise from the intermittent, turbulent nature of the interplanetary magnetic field, causing magnetic reconnection to occur at the magnetopause on a wide range of spatial and temporal scales.

- The multiscale ionospheric velocity data are not consistent with a simple single LR circuit model often used to describe the open magnetosphere. Instead, we suggest that they are consistent with a multiscale reconnection model incorporating a number of LR circuits with a range of spatial and temporal scales.

[50] **Acknowledgments.** We are grateful to the principle investigator of the Finland (CUTLASS) SuperDARN radar, M. Lester. CUTLASS is supported by the Particle Physics and Astronomy Research Council, UK, the Swedish Institute for Space Physics, and the Finnish Meteorological Institute Helsinki. We are grateful to the IMAGE PI institute, the Technical University of Braunschweig, Germany. The IMAGE magnetometer data are collected as a Finnish-German-Norwegian-Polish-Russian-Swedish project. We would like to thank K. A. McWilliams for the data plotted in Figure 1 and for providing the list of PIF intervals. We would also like to thank N. W. Watkins and G. Chisham for helpful discussions.

[51] Arthur Richmond thanks Stephan C. Buchert and G. Provan for their assistance in evaluating this paper.

## References

- Bering, E. A., III, J. R. Benbrook, G. J. Byrne, B. Liao, J. R. Theal, L. J. Lanzerotti, and C. G. MacLennan, Balloon measurements above the South Pole: Study of ionospheric transmission of ULF waves, *J. Geophys. Res.*, *100*, 7807–7819, 1995.
- Bristow, W. A., and R. A. Greenwald, On the spectrum of thermospheric gravity waves observed by the Super Dual Auroral Radar Network, *J. Geophys. Res.*, *102*, 11,585–11,595, 1997.
- Buchert, S. C., R. Fujii, and K.-H. Glassmeier, Ionospheric conductivity modulation in ULF pulsations, *J. Geophys. Res.*, *104*, 10,119–10,133, 1999.
- Burlaga, L. F., *Interplanetary Magnetohydrodynamics*, chapter 9, Oxford Univ. Press, New York, 1995.
- Campbell, W. H., An analysis of the spectra of geomagnetic variations having periods from 5 min to 4 hours, *J. Geophys. Res.*, *81*, 1369–1390, 1976.
- Chisham, G., and M. Pinnock, Assessing the contamination of SuperDARN global convection maps by non-F-region backscatter, *Ann. Geophys.*, *20*, 13–28, 2002.
- Consolini, G., P. De Michelis, A. Meloni, L. Cafarella, and M. Candidi, Levy-stable probability distribution of magnetic field fluctuations at Terra Nova Bay (Antarctica), in *Proc. Italian Res. On Antarctic Atmosphere*, pp. 367–376, Soc. Ital. di Fisica, Bologna, Italy, 1998.
- Fasel, G. J., Day side poleward moving auroral forms: A statistical study, *J. Geophys. Res.*, *100*, 11,891–11,905, 1995.

- Francia, P., U. Villante, and A. Meloni, An analysis of geomagnetic field variations (3 min-2 h) at a low latitude observatory ( $L = 1.6$ ), *Ann. Geophys.*, *13*, 522–531, 1995.
- Freeman, M. P., N. W. Watkins, and D. J. Riley, Evidence for a solar wind origin of the power law burst lifetime distribution of the AE indices, *Geophys. Res. Lett.*, *27*, 1087–1090, 2000a.
- Freeman, M. P., N. W. Watkins, and D. J. Riley, Power law distributions of burst duration and interburst interval in the solar wind: Turbulence or dissipative self-organized criticality, *Phys. Rev. E*, *62*, 8794–8797, 2000b.
- Goldstein, M. L., and D. A. Roberts, Magnetohydrodynamic turbulence in the solar wind, *Phys. Plasmas*, *6*, 4154–4160, 1999.
- Greenwald, R. A., et al., DARN/SuperDARN: A global view of the dynamics of high-latitude convection, *Space Sci. Rev.*, *71*, 761–796, 1995.
- Holzer, T. E., and G. C. Reid, The response of the dayside magnetosphere-ionosphere system to time-varying field line reconnection at the magnetopause: Theoretical model, *J. Geophys. Res.*, *80*, 2041–2056, 1975.
- Kuo, H., C. T. Russell, and G. Le, Statistical studies of flux transfer events, *J. Geophys. Res.*, *100*, 3513–3519, 1995.
- Lockwood, M., and M. N. Wild, On the quasi-periodic nature of magnetopause flux transfer events, *J. Geophys. Res.*, *98*, 5935–5940, 1993.
- Lühr, H., A. Aylward, S. C. Buchert, A. Pajunpää, K. Pajunpää, T. Holmboe, and S. M. Zalewski, Westward moving dynamic substorm features observed with the IMAGE magnetometer network and other ground-based instruments, *Ann. Geophys.*, *16*, 425–440, 1998.
- McWilliams, K. A., T. K. Yeoman, and G. Provan, A statistical survey of dayside pulsed ionospheric flows as seen by the CUTLASS Finland HF radar, *Ann. Geophys.*, *18*, 445–453, 2000.
- Provan, G., and T. K. Yeoman, Statistical observations of MLT, latitude and size of pulsed ionospheric flows with the CUTLASS Finland radar, *Ann. Geophys.*, *17*, 17,855–17,867, 1999.
- Reiff, P. H., R. W. Spiro, and T. W. Hill, Dependence of polar cap potential drop on interplanetary parameters, *J. Geophys. Res.*, *86*, 7639–7648, 1981.
- Roberts, D. A., and M. L. Goldstein, Turbulence and waves in the solar wind, *Rev. Geophys.*, 932–943, 1991.
- Sanchez, E. R., G. L. Siscoe, and C. I. Meng, Inductive attenuation of the transpolar voltage, *Geophys. Res. Lett.*, *18*, 1173–1176, 1991.
- Schroeder, M. R., *Fractals, Chaos, Power Laws*, chapter 5, W.H. Freeman, New York, 1991.
- Takalo, J., and J. Timonen, Characteristic time scale of auroral electrojet data, *Geophys. Res. Lett.*, *21*, 617–620, 1994.
- Tsurutani, B. T., M. Sugiura, T. Iyemori, B. E. Goldstein, W. D. Gonzalez, S. I. Akasofu, and E. J. Smith, The nonlinear response of AE to the IMF  $B_S$  driver: A spectral break at 5 hours, *Geophys. Res. Lett.*, *17*, 279–282, 1990.
- Watkins, N. W., Scaling in the space climatology of auroral indices: Is SOC the only answer?, *Nonlinear Proc. Geophys.*, *9*, 389–398, 2002.
- Weatherwax, A. T., J. T. Rosenberg, L. J. Lanzerotti, C. G. MacLennan, H. U. Frey, and S. B. Mende, The distention of the magnetosphere on May 11, 1999: High latitude Antarctic observations and comparisons with low latitude magnetic and geopotential data, *Geophys. Res. Lett.*, *27*, 4029–4032, 2000.
- Weimer, D. R., C. K. Goertz, D. A. Gurnet, N. C. Maynard, and J. L. Burch, Auroral zone electric fields from DE1 and 2 at magnetic conjunction, *J. Geophys. Res.*, *90*, 7479–7494, 1985.

---

G. A. Abel and M. P. Freeman, British Antarctic Survey, High Cross, Madingley Road, Natural Environment Research Council, Cambridge, CB3 0ET, U.K. (gaab@bas.ac.uk; mpf@bas.ac.uk)